Journal of Geophysical Research: Atmospheres

RESEARCH ARTICLE
10.1029/2018JD029013

Key Points:
- BC concentrations increased as a result of the enhanced convergence due to an intraseasonal anomalous lower-level cyclone development
- The increased concentrations of BC warm the atmosphere due to the absorption of radiation and enhance the lower-level cyclone
- The study illustrates that more realistic prediction of short-term atmospheric changes should consider the coupling of aerosols-circulation

Correspondence to:
J. Yang,
yangjing@bnu.edu.cn

Citation:
Yang, J., Wang, W.-C., Chen, G., Bao, Q., Qi, X., & Zhou, S. (2018). Intraseasonal variation of the black carbon aerosol concentration and its impact on atmospheric circulation over the southeastern Tibetan Plateau. *Journal of Geophysical Research: Atmospheres*, *123*, 10,881–10,894. https://doi.org/10.1029/2018JD029013

Received 15 MAY 2018
Accepted 17 SEP 2018
Accepted article online 19 SEP 2018
Published online 8 OCT 2018

Author Contributions:
Conceptualization: Jing Yang, Wei-Chyung Wang
Data curation: Jing Yang
Formal analysis: Jing Yang
Funding acquisition: Jing Yang
Investigation: Jing Yang
Methodology: Jing Yang, Guoxing Chen, Qing Bao
Resources: Jing Yang
Supervision: Jing Yang, Wei-Chyung Wang
Validation: Jing Yang
Visualization: Jing Yang
Writing - original draft: Jing Yang
Writing – review & editing: Jing Yang

Intraseasonal Variation of the Black Carbon Aerosol Concentration and Its Impact on Atmospheric Circulation Over the Southeastern Tibetan Plateau

Jing Yang[1,2], Wei-Chyung Wang[2], Guoxing Chen[2], Qing Bao[3], Xin Qi[1], and Siyuan Zhou[1]

[1]State Key Laboratory of Earth Surface Processes and Resource Ecology (ESPRE)/Academy of Disaster Reduction and Emergency Management Ministry of Civil Affairs and Ministry of Education, Faculty of Geographical Science, Beijing Normal University, Beijing, China, [2]Atmospheric Sciences Research Center, State University of New York at Albany, Albany, NY, USA, [3]State Key Laboratory of Numerical Modeling for Atmospheric Sciences and Geophysical Fluid Dynamics (LASG), IAP/CAS, Beijing, China

Abstract The black carbon (BC) concentration over the southeastern Tibetan Plateau is modulated by atmospheric intraseasonal variations and in turn affects atmospheric circulation through both direct radiative atmospheric warming and surface cooling. Based on an intraseasonal dry-wet phase transition over the southeastern Tibetan Plateau, we investigated the short-term radiative-dynamic coupling of the atmosphere with changes in the concentration of BC using both observations and numerical sensitivity experiments. The observed local concentrations of BC increased by >50% as a result of the enhanced convergence and upward migration associated with the development of an intraseasonal anomalous lower-level cyclone. Calculations using an offline radiation transfer model showed that this increase in BC concentration led to ~4 W/m^2 of atmospheric radiative warming and ~2 W/m^2 of surface radiative cooling. Consequently, an anomalous lower-level cyclone with an average wind speed of 0.5 m/s (~10% of the natural change from a dry to a wet phase) developed in a linear baroclinic model and an aerosol-aware WRF model, which was mainly a result of the atmospheric warming while the surface cooling played only a minor role. Although the change in precipitation was small, cloud fraction was significantly increased due to the enhanced upward motion in the atmosphere. This warrants further studies of cloud adjustments to the BC concentration on both cloud fraction and microphysics aspects. The present study illustrates that consideration of aerosol-circulation coupling is imperative to advance the subseasonal prediction of atmospheric circulation.

Plain Language Summary The present study illustrates that consideration of aerosol-circulation coupling is imperative to advance the subseasonal prediction of atmospheric circulation.

1. Introduction

The Tibetan Plateau (TP), with its high mean elevation of >4,500 m, has a significant influence on atmospheric circulation through local thermal forcing (Wu et al., 2015; Yeh et al., 1957). For example, Liu et al. (2007) showed that the diabatic heating caused by the TP in summer enhances the development of anticyclones in the upper troposphere over the TP and produces an intraseasonal oscillation. Intraseasonal variations (ISVs) dominate the variation in dry-wet conditions over the TP in summer (Endo et al., 1994; Yamada & Uyeda, 2006; Zhan & Li, 2008), which, in turn, strongly affect the initiation and development of drought and flooding in the downstream Asian monsoon region during the boreal summer (Duan et al., 2012; Tao & Ding, 1981). Therefore, an understanding of ISVs on the TP is crucial in improving the extended range forecast for both local and downstream regions.

The ISV is particularly strong for precipitation over the southeastern TP (SETP; see Figure 1 in Yang et al., 2016), where the circulation anomaly is characterized by a developing lower-level cyclone (LLC) during the transition from dry to wet spells. In its developing phase over the SETP, the LLC is initiated by the prewarming of lower levels of the atmosphere and is subsequently enhanced by midlevel latent heating (Yang et al., 2016), which is essentially caused by perturbations of the wave train in midlatitude and/or lower latitudes

(Hu et al., 2016; Wang & Duan, 2015). The anomalous LLC is usually accompanied by strong upward motion of the local atmosphere and lower-level atmospheric convergence (Yang et al., 2016; Zhang et al., 2014), which is likely to transport atmospheric pollutants from surrounding regions.

The areas surrounding the TP have become hot spots for black carbon (BC) emissions in recent decades (Xia et al., 2011). The prevailing southwesterly/southeasterly winds transport BC aerosols to the TP from northern India (Zhao et al., 2013), western and central China (Kopacz et al., 2011; Ming et al., 2009) and Nepal, the Middle East, Pakistan, and other countries (Bucci et al., 2014; Li et al., 2016). Because BC strongly absorbs shortwave radiation, previous studies have mainly concentrated on the long-term climatic effects of BC, such as increasing radiative heating of the atmosphere (He et al., 2014; Lau et al., 2006) or reducing the albedo of snow (Kopacz et al., 2011; Lee et al., 2016; Qian et al., 2011). Lau et al. (2006, 2010) proposed the elevated heat pump hypothesis, which posits that atmospheric heating by deep layers of BC accumulated over the Himalayan foothills may lead to increased precipitation in the foothills during the early monsoon season (from early June to mid-July). However, there have been few studies of the shorter-term (intraseasonal and synoptic) modulating effects of BC on atmospheric circulation over the TP.

There have been several studies on the meteorological impact of aerosol loading on intraseasonal timescales. Aerosols can be modulated by the Madden-Julian oscillation, which is a typical intraseasonal oscillation in tropical regions (Tian et al., 2008). There have also been many modeling studies on the impact of aerosols on meteorology—for example, aerosols may affect atmospheric circulation in the transition from breaks in the Indian monsoon to active spells (Manoj et al., 2011), as well as the development of cyclones in northern America (Thompson & Eidhammer, 2014). Coupling and feedback have often been implied in these previous studies, but without a clean demonstration of the effects.

This study investigated short-term aerosol-circulation coupling based on an intraseasonal rainfall event. We studied the characteristics of the BC spatial distribution changes associated with the quasi-9-day ISV circulation, its radiative forcing, and its feedback on circulation over the SETP in summer. The study is limited to the direct radiative effects of BC and the coupling of BC-cloud microphysics, whereas the effect of BC on the surface albedo is not included.

Section 2 introduces the data sets and model description. Section 3 describes spatial distribution change of BC concentration during the ISV and the associated changes in circulation using reanalysis meteorological and aerosol data sets. Section 4 illustrates BC effects on the circulation, which is estimated through three-stage numerical simulations using an offline radiation transfer model, a linear baroclinic model (LBM), and an aerosol-aware WRF (Weather Research and Forecasting) model, and the conclusion and discussion are given in section 5.

2. Data Sets and Models

2.1. Data Sets

We use daily rainfall data sets from the 0.25° × 0.25° gridded stations of the China Meteorological Administration (Wu & Gao, 2013). The daily circulation data are retrieved from the European Centre for Medium-Range Weather Forecasts ERA-Interim data set (Dee et al., 2011; Simmons et al., 2007) at a resolution of 1.5° × 1.5° (http://dataportal.ecmwf.int/data/d/interim_daily/). Because BC measurements are unavailable for our case study, MACC-II (Monitoring Atmospheric Composition and Climate Interim Implementation; Peuch et al., 2014) aerosol reanalysis data sets from the European Centre for Medium-Range Weather Integrated Forecasting System (Benedetti et al., 2009; Morcrette et al., 2009) are used to provide the three-dimensional BC concentrations (mixing ratio kg/kg) and the aerosol optical depth (AOD). The MACC-II data sets have a horizontal resolution of 1° × 1° and a vertical resolution of 60 levels at 6-hr intervals. The BC emissions are primarily from the Global Fire Emission Database, Speciated Particulate Emissions Wizard, and Emission Database for Global Atmospheric Research data sets. To verify the change in the distribution of BC, we also examine our results using the Second Modern-Era Retrospective Analysis for Research and Applications (Molod et al., 2015) reanalysis data set produced by the Goddard Earth Observing System version 5 (Rienecker et al., 2008) using the Goddard Chemistry, Aerosol, Radiation, and Transport (Chin et al., 2002) model. The two data sets give very similar results. We selected a case study from summer 2008 because aerosol reanalysis data sets are more reliable after 2006 with the inclusion of more satellite observations.

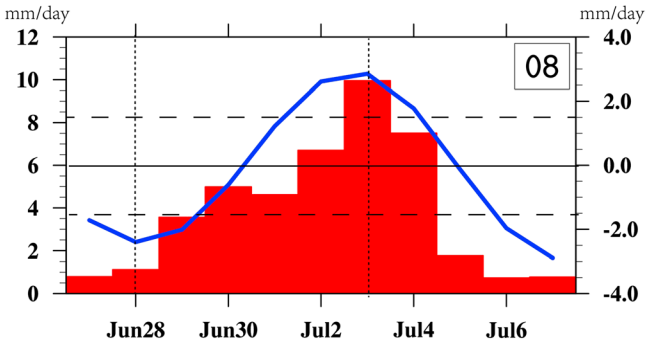

Figure 1. Time series of total (red bar, scale on left-hand *y*-axis) and filtered (blue line, scale on right-hand *y*-axis) rainfall averaged over the southeastern Tibetan Plateau core region (28–34° N, 90–100° E) in the quasi-9-day rainfall event in summer 2008. The two dotted black lines show the peak dry date (28 June 2008) and the peak wet date (3 July 2008), and the two dashed black lines mark 1 standard deviation of summer rainfall. Units: mm/day.

2.2. Model Description

We used three numerical models to simulate the BC effects in different stages. First, an offline radiation transfer package calculates the directive radiative forcing associated with BC changes during an ISV events, then the calculated radiate forcing is incorporated into the LBM to estimate the first-order effect on the circulation, and lastly, simulations with an aerosol-aware WRF model are to provide a more-realistic perspective of circulation changes caused by the BC variation. All three models are briefly introduced below, and details on the experiment setup are given in section 4 for each individual model.

The offline radiation transfer package is constructed based on the RRTMG (the rapid radiation transfer models for application to general circulation models) shortwave and longwave radiation schemes (Iacono et al., 2008) in the WRF model. It reads meteorological fields (including atmospheric profiles and surface properties) from the WRF output and the prescribed multiple-component aerosol fields (including sulfate, organic carbon, BC, sea salt, and dust) and then calculates the radiative properties of aerosols using subroutines imported from the WRF-Chem Model.

We use a dry version of the global, time-dependent, and primitive equation LBM (Watanabe & Kimoto, 2000). The LBM has been built up to examine linear dynamics in the atmosphere—for example, to compute a steady linear response to prescribed forcing. It facilitates an understanding of complicated feedback by giving a pure linear response of the atmospheric circulation to specific heating profiles over specific domains in the dynamic atmosphere. We purposely remove the moisture process in order to identify the circulation response to prescribed BC induced radiative effects.

The aerosol-aware WRF, based on the WRF model version 3.6.1, includes online simulation of aerosol direct and indirect effects using prescribed multicomponent aerosol fields (Chen et al., 2017). Similar to the offline radiation transfer package, it calculates the radiative properties of aerosols using subroutines imported from the WRF-Chem Model. Soluble aerosol species (sulfate and sea salt) are converted into equivalent ammonium sulfate based on their hygroscopicity and serve as cloud nuclei in a two-moment cloud microphysical scheme (Chen et al., 2015; Chen & Wang, 2016; Cheng et al., 2007, 2010) to account for aerosol-cloud-radiation interactions. We fixed the equivalent amount of ammonium sulfate to exclude the effect of aerosols on the cloud nuclei. Therefore, in this study, the WRF model includes the radiative effects of BC and cloud adjustments to take account of changes in the meteorological conditions but does not include the microphysical interactions of BC with clouds. The other physical processes are configured using the Kain-Fritsch scheme (Kain, 2004) for cumulus convection, the Noah scheme (Chen & Dudhia, 2001) for land surface interactions, the Monin-Obukhov scheme (Monin & Obukhov, 1954) for the surface layer, and the Yonsei University scheme (Hong et al., 2006) for the planetary boundary layer.

The horizontal resolution of the WRF model in this study is 15 km with 49 vertical levels. The model is driven by meteorological forcing from the ERA-Interim Reanalysis data set, and the sea surface temperature is fixed throughout the simulation. The aerosol data sets are taken from the MACC-II and Second Modern-Era Retrospective Analysis for Research and Applications data sets. The simulation domain of WRF covers the region between 21–42°N and 80–112°E (shown in Figure 5). The refractive index of BC keeps constant as 1.95 + 0.79i throughout the simulation so that the BC aging process is not included. Only the BC concentrations change in the numerical experiments, and the concentrations of sea salt, dust, organic carbon, and sulfate remain unchanged. This study applied the WRF model to investigate the effect of BC on short-term changes in circulation by inputting two types of prescribed BC distributions.

3. Changes in BC Concentrations With ISVs on the SETP

3.1. The ISV Event and Associated Circulation Features

In a similar manner to Yang et al. (2014, 2016), we used two criteria to identify a typical ISV event of rainfall over the SETP: (1) The absolute amount of maximum/minimum amplitude anomaly in the wet/dry phase exceeds 1 standard deviation of the time series of the summer (June-July-August) intraseasonal

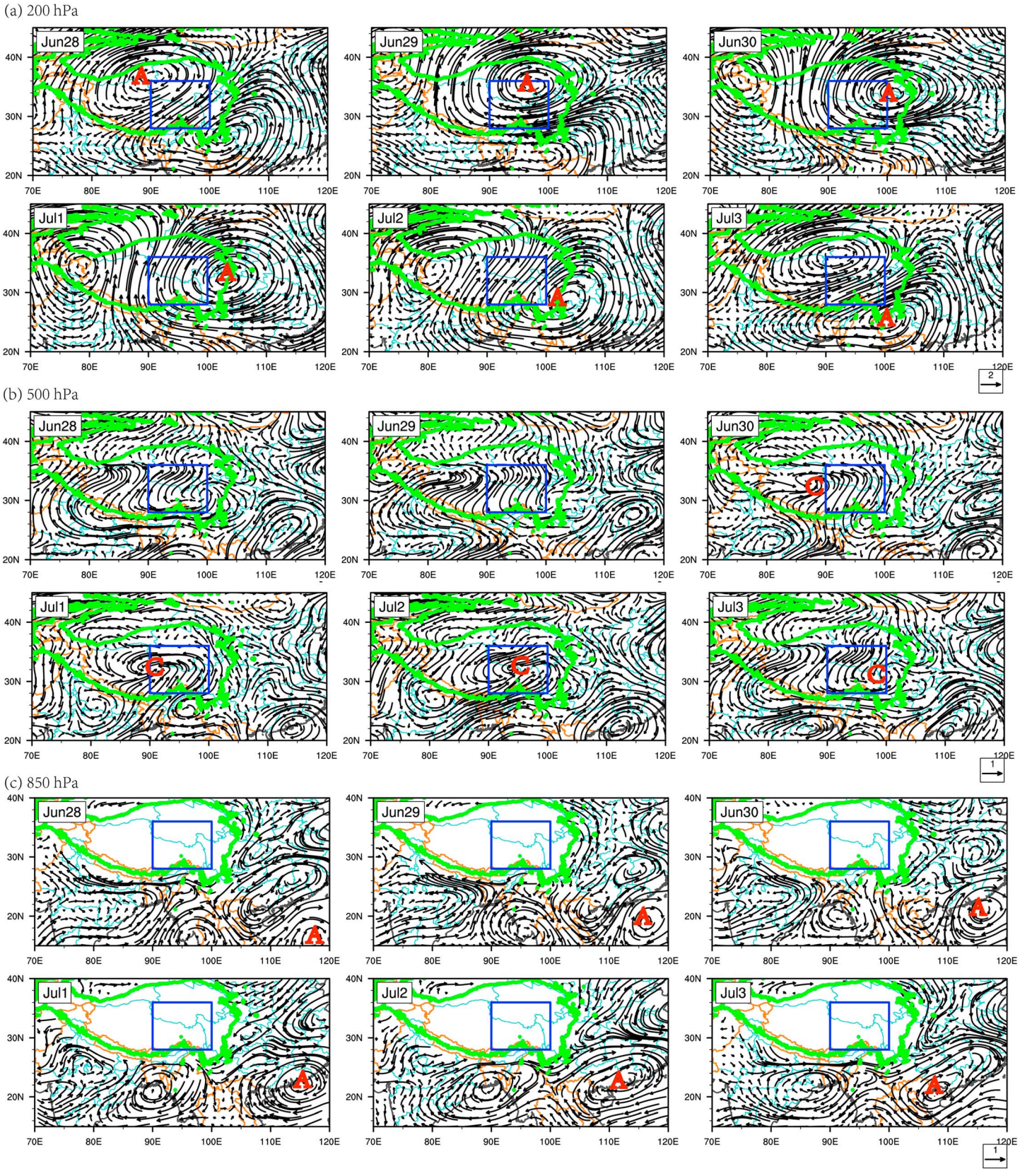

Figure 2. Spatial evolution of the quasi-9-day component winds from the peak dry date to the peak wet date at (a) 200, (b) 500, and (c) 850 hPa. Units: m/s. The letter C denotes the cyclonic anomaly, and the letter A denotes the anticyclonic anomaly.

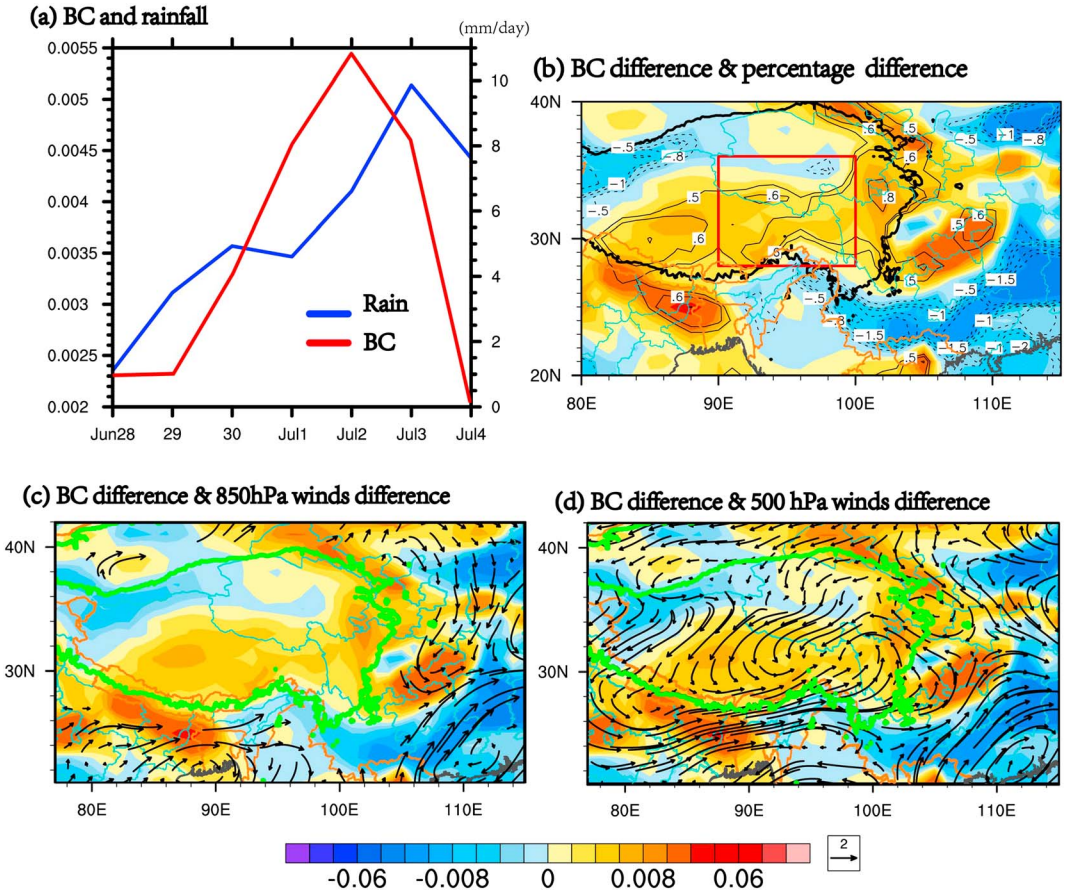

Figure 3. (a) Time series of the aerosol optical depth (AOD) of BC (red line) and the total rainfall (blue line, units: Mm day^{-1}) averaged over the southeastern Tibetan Plateau core region (red box in part (b), 28–34° N, 90–100° E) at the transition period of the quasi-9-day event. (b) Difference in spatial distribution between the maximum amount of BC (2 July 2008) and minimum amount of BC (28 June 2008) for the absolute AOD (shading) and fractional percentage AOD (contours). (c and d) Differences in spatial distribution between the maximum amount of BC (2 July 2008) and minimum amount of BC (28 June 2008) for the absolute AOD (shading) and the winds at 850 and 500 hPa (vectors, units: m/s). The blue boxes in represent southern and eastern areas of the TP. BC = black carbon.

component, and (2) both the peak-wet and peak-dry phases in the ISV event can be clearly identified in the time series of total rainfall. Based on previous studies, one of the most dominant ISVs is a quasi-9-day periodicity over SETP. This anomaly is extracted based on Fourier harmonic analysis (see Yang et al., 2010, 2014). The rainfall averaged over the core domain (28–34°N, 90–100°E) is chosen as a representative variable to distinguish the ISVs over the SETP. Using these approaches, a typical quasi-9-day event over the SETP from 28 June to 6 July 2008 is selected for this study (Figure 1a). Within this cycle, a transition from a peak dry to a peak wet phase is defined as the period from 28 June to 3 July 2008.

We next attempt to recognize the evolution of the circulation in this transition phase. Figures 2a–2c show the evolution of the quasi-9-day component of circulation in the upper, middle, and lower levels of the atmosphere, respectively. An anticyclonic anomaly propagates southeast from the northwestern TP to the SETP roughly along the westerly jet in the upper level of the atmosphere (Figure 2a) and an anticyclonic anomaly propagates northwest from the western Pacific to southeastern China at lower levels (Figure 2c). An anomalous, well-organized LLC (i.e., convergence) gradually develops over the SETP at lower levels (500 hPa, Figure 2b) from the peak dry to the peak wet phase. This is the most distinguishable circulation anomaly in this transition and is accompanied by strong ascending motion over the SETP and lower-level convergence toward the SETP (see Figure 12 in Yang et al., 2016). These features are consistent with the behavior of the typical quasi-9-day mode described by Yang et al. (2016). Thus, this selected case study can be considered as representative of the ISV over the SETP. This transition from a dry to a wet phase (the first half-cycle of the ISV) is the focus of this study because the LLC formed during this transition and probably drove the convergence of BC toward the TP.

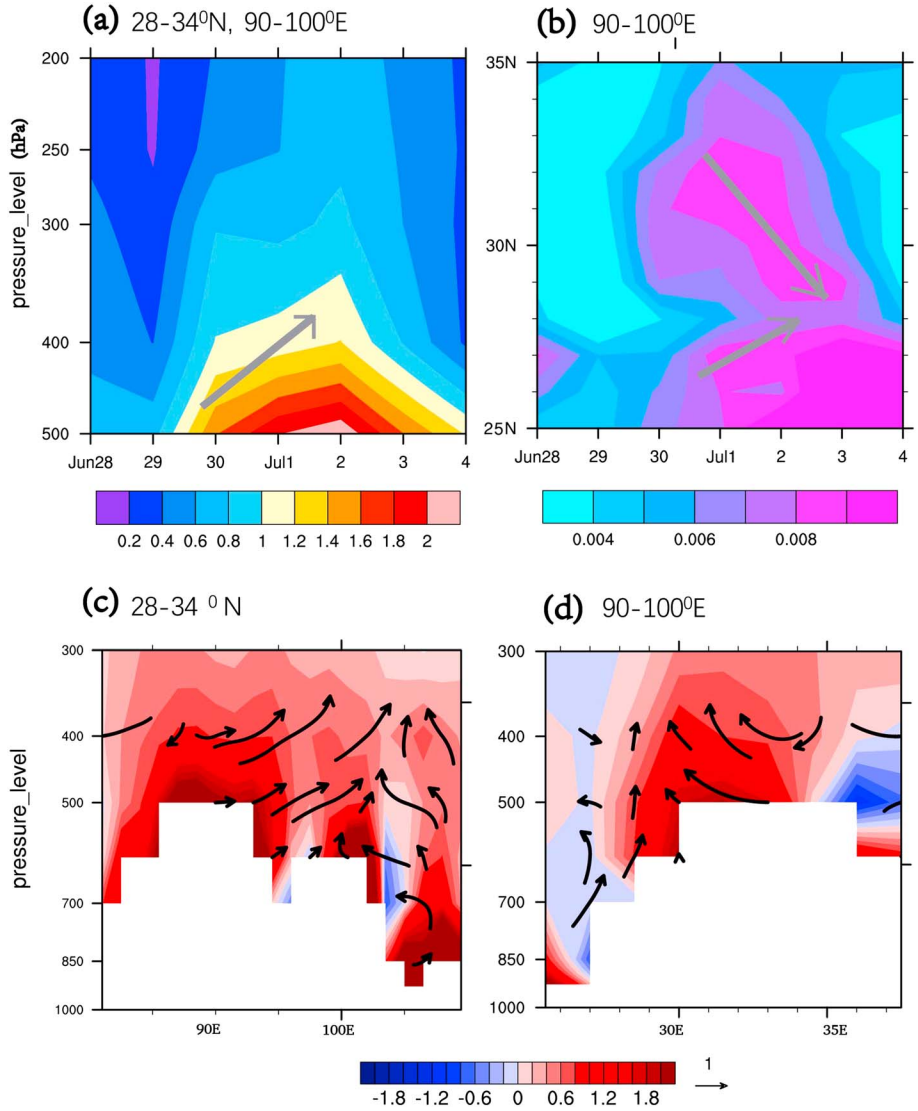

Figure 4. (a) Time (*x*-axis)-pressure (*y*-axis: hPa) diagram averaged over the core region of the southeastern Tibetan Plateau (28–34° N, 90–100° E) for a black carbon (BC) concentration of 10^{-10} kg/kg). (b) Time (*x*-axis)-latitude (*y*-axis) diagram averaged between 90° and 100° E for the AOD of BC. (c) Vertical cross section of BC concentration (10^{-10} kg/kg) and winds, averaged along 28–34° N. d vertical cross section for the concentration of BC (10^{-10} kg/kg) and winds (m/s) averaged along 90–100°E. The vertical velocity is expanded 10 times. The gray solid arrows in (a) and (b) represent the direction of propagating of the BC.

3.2. Changes in BC Concentrations Related to the ISV Event

A comparison of the time series of the AOD of BC and the average rainfall over the SETP core region showed that the variation in BC was not in phase with the variation in rainfall during the transition phase: the peak phase of BC led the peak wet phase by 1 day (Figure 3a). This inconsistency in the variation of BC and rainfall may be caused by heavy washout due to rainfall decreasing the BC concentration during the peak wet phase over the SETP core region. BC has minimum concentrations at 28 June and maximum concentrations at 2 July over SEPT. Figure 3b shows the spatial variation in the BC AOD between the maximum and minimum phases. Compared with the BC minimum phase, BC in its maximum phase significantly increases by >50% over the southern and eastern TP, southwestern China (the Sichuan Basin), and the southwest and northeast flanks of the TP. The regions where the concentrations evidently increase, including the eastern and southern TP (blue squares in Figure 3), are consistent with those in which the LLC anomaly (convergence) occurs

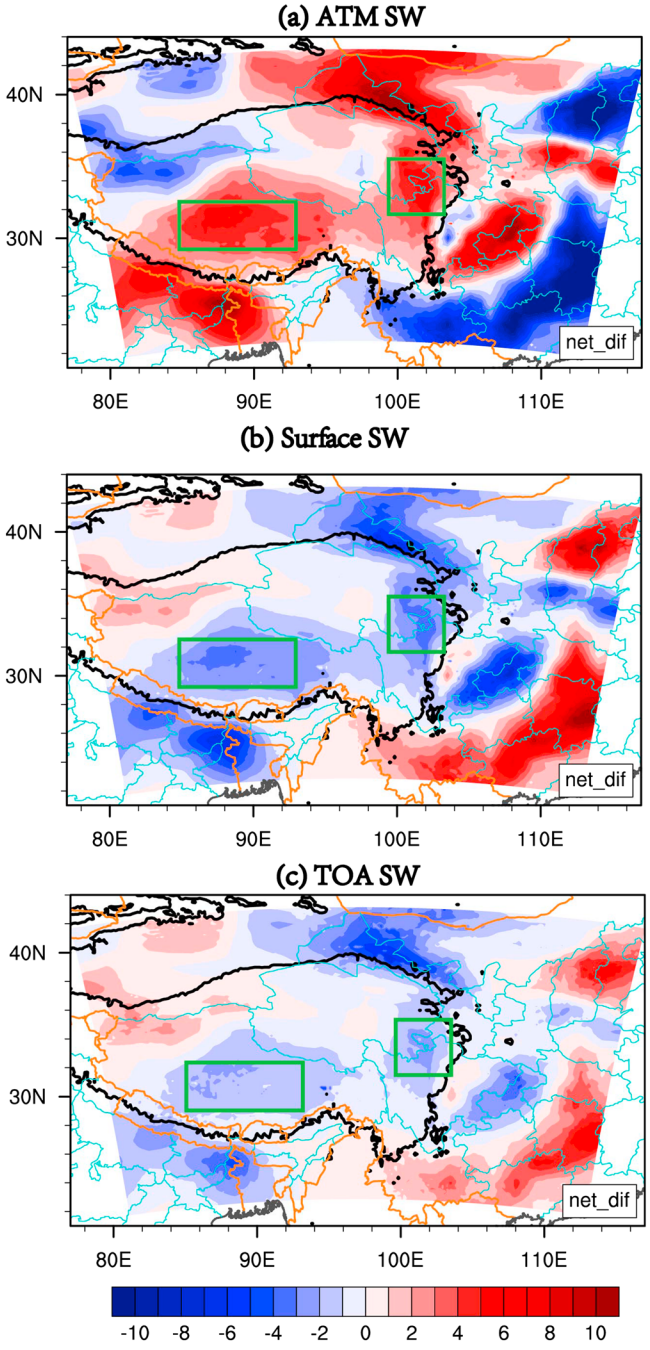

Figure 5. Spatial differences between the maximum and minimum runs of RRTMG for black carbon for shortwave radiation (W/m^2) (a) within the atmospheric column, (b) at the surface, and (c) at the top of the atmosphere. The green boxes represent the southern and eastern Tibetan Plateau.

(Figures 3c and 3d). The southern and eastern TP are two subregions where there is a maximum increase in BC with regional changes in the AOD up to a maximum of 0.012.

The BC concentration over the SETP core region experiences an evident upward migration during this transition (Figure 4a), which corresponds to local upward motion of the atmosphere (Figures 4c and 4d). There is a noticeable meridional convergence of the BC concentrations (Figure 4b) corresponding to a convergence of the lower-level meridional circulation (Figures 3c and 3d). Therefore, the variation in BC concentration is closely related to the corresponding variation in the circulation in the lower-middle atmosphere during this transition. These major characteristics are also clearly seen in the MERRA-2 data set, where there is no daily variation in BC emissions. There may be uncertainties in the magnitude of the BC reanalysis (Myhre et al., 2013; Samset et al., 2013), but we are currently unable to access more reliable observational data sets for this case study.

4. Radiation-Circulation Interactions

We estimate the radiative forcing caused by changes in BC concentration using an offline radiation transfer package and then simulate the induced meteorological feedback (circulation, cloud, and rainfall) using the WRF model. We use an LBM to facilitate our understanding of the changes in circulation in the WRF model simulations. To better recognize the short-term feedback on circulation with different spatial distributions of BC, the numerical study uses idealized sensitivity experiments with two contrasting prescribed BC distributions at the times of BC minimum (28 Jun) and maximum (6 Jul) concentration, rather than the real day-by-day variation in BC concentrations.

4.1. Radiative Forcing

Using the described offline radiation transfer model, radiative forcing is determined by the differences in total shortwave and longwave radiation between two sets of BC distributions, representative of the minimum BC concentrations over the SETP on 28 June 2008 (BC minimum run) and the maximum BC concentration over the SETP on 2 July 2008 (BC maximum run). Only the concentrations of BC change, while the concentrations of sea salt, dust, organic carbon, and sulfate remain unchanged from the values on 28 June 2008. We examine the sensitivity of the results to different meteorological conditions in the RRTMG scheme using the meteorological background in extreme dry and extreme wet phases. The results show that almost similar radiative forcing patterns are caused by changes in the BC concentrations. Therefore, radiative forcing is not sensitive to the meteorological conditions in this case study and the calculations are based on the atmospheric conditions on 28 June 2008.

Because the calculated longwave forcing is 1 to 2 orders of magnitude smaller than the shortwave forcing, Figure 5a shows the clear sky shortwave radiative forcing within the atmospheric column at the surface and at the top of the atmosphere (TOA). Consistent with the variation in the spatial distribution of BC (Figure 3), positive shortwave forcing on the atmosphere is found over the southern and eastern TP, southwestern China, and the southwest and northeast flanks of the TP. Figures 5b and 5c show that shortwave forcing over these regions is negative at both the surface (downward) and at the TOA (upward). We further calculate the amount of domain-averaged shortwave forcing caused by variations in the concentration of BC over the southern (29–33°N, 85–93°E) and eastern (31–35°N, 100–104°E) TP. Within the atmosphere, the area-averaged shortwave forcing is about 3.6 W/m^2 over the southern TP and 4.3 W/m^2 over the eastern

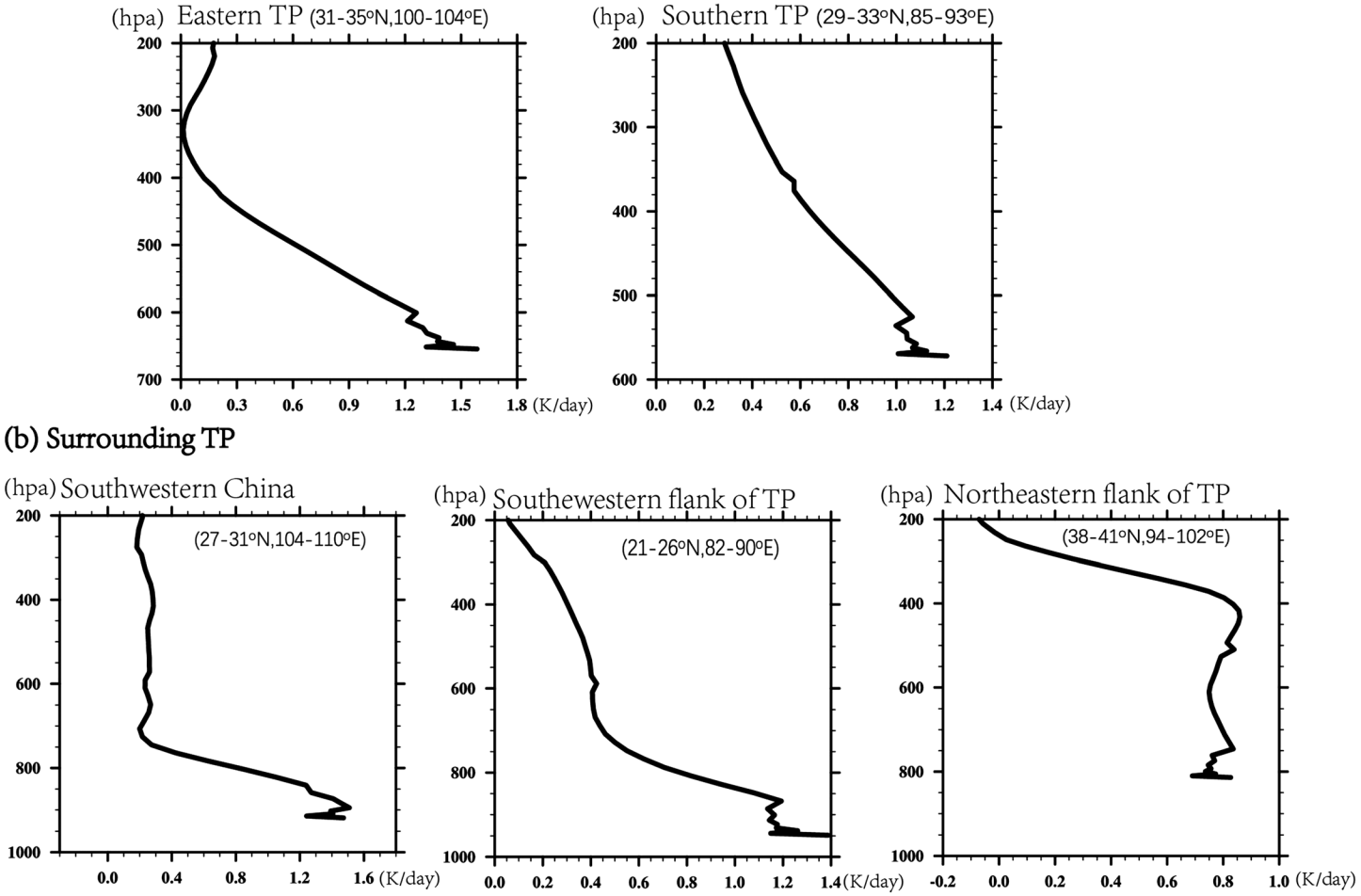

Figure 6. Differences in black carbon radiative heating rate profiles (K/day) over the five major domains over the TP and its surrounding regions from RRTMG as shown in Figure 7. TP = Tibetan Plateau.

TP. At the surface, the area-averaged shortwave forcing is nearly -2.4 W/m^2 over the southern TP and -2.6 W/m^2 over the eastern TP. At the TOA, the area-averaged shortwave forcing is -1.2 W/m^2 over the southern TP and -1.7 W/m^2 over the eastern TP. The above forcing amplitudes are comparable with some previous studies (Kopacz et al., 2011; Zhuang et al., 2013), which is purely induced by BC radiative effect.

Figure 6 shows the area-averaged vertical profile of atmospheric heating over the five domains. The whole air column becomes warmer, particularly at lower levels. The maximum heating rate over the eastern and southern TP can reach up to >1.2 K/day at lower levels. This rate of heating over the TP is considerable because the density and pressure over the TP are much smaller than over the surrounding regions.

4.2. Changes in Circulation

4.2.1. LBM Simulations

We carried out six experiments to investigate the circulation response to BC radiative heating. The first five experiments are forced by BC radiative heating respectively over the five regions, the southern TP, eastern TP, southwestern China, the southwestern flank of the TP, and the northeastern flank of the TP according to their heating profiles from the RRTMG scheme (Figure 6). The sixth experiment is forced by a total of five heating profiles. We focus here on the response of the lower atmosphere to the heating forces. Figures 7a–7e show the response of the circulation to each heating profile at 500 hPa, which is used to represent the lower

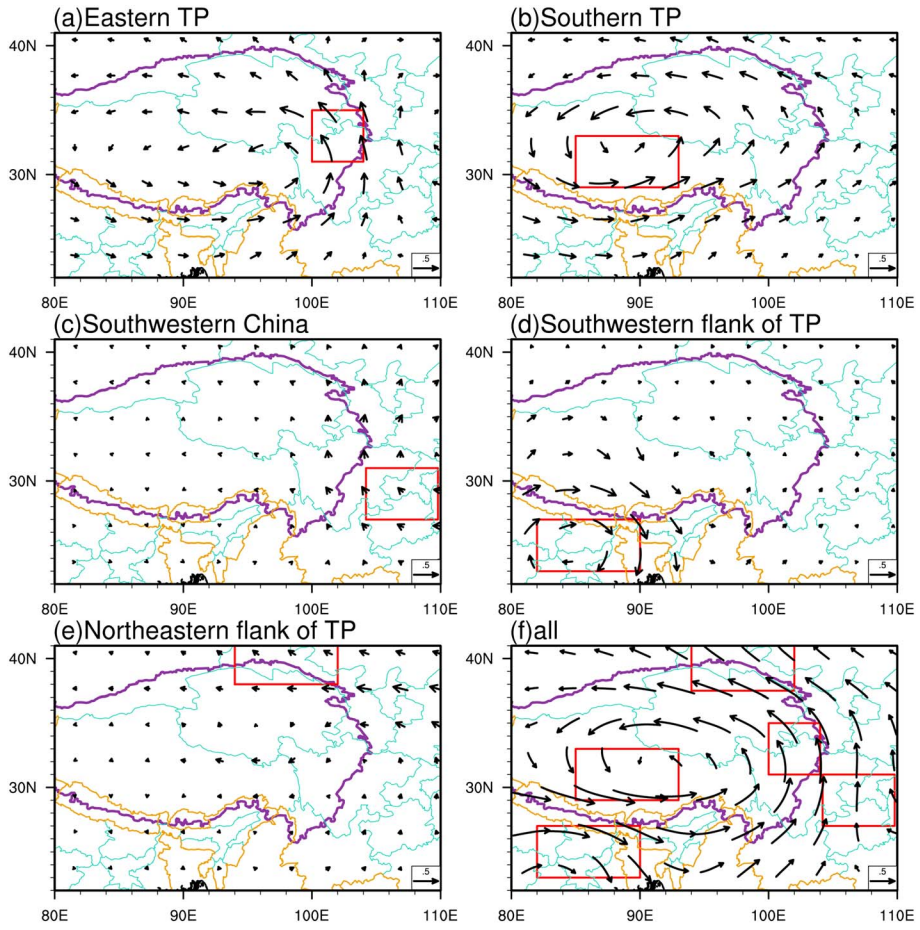

Figure 7. Responses of 500 hPa circulation to heating profiles over five specific domains in the LBM simulation (units: m/s). The red box represents the location of heat forcing, as in Figure 6. LBM = linear baroclinic model; TP = Tibetan Plateau.

level of the atmosphere over the TP. Consistent with the thermal adaptation theory of the atmosphere (Wu et al., 2009), the radiative forcing by BC over both the southern and eastern TP can directly produce a clear local LLC anomaly over the TP region (Figures 7a and 7b). Other heating forces over the surrounding regions of the TP do not cause significant anomalies over the TP at lower levels (Figures 7c–7e). Correspondingly, the joint response of the circulation forced by total heating over these five domains is a remarkable LLC over the SETP (Figure 7f), which indicates that heating by BC over the southern and eastern TP plays a major part in changing the circulation over the TP.

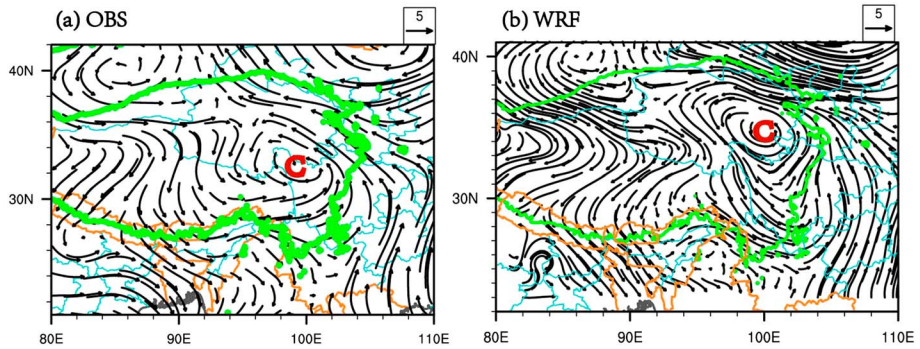

Figure 8. Differences in the circulation at 500 hPa between the maximum (2 July 2008) and minimum (28 June 2008) concentrations in (a) the observations and (b) the WRF simulation (units: m/s). OBS = observed; WRF = Weather Research and Forecasting.

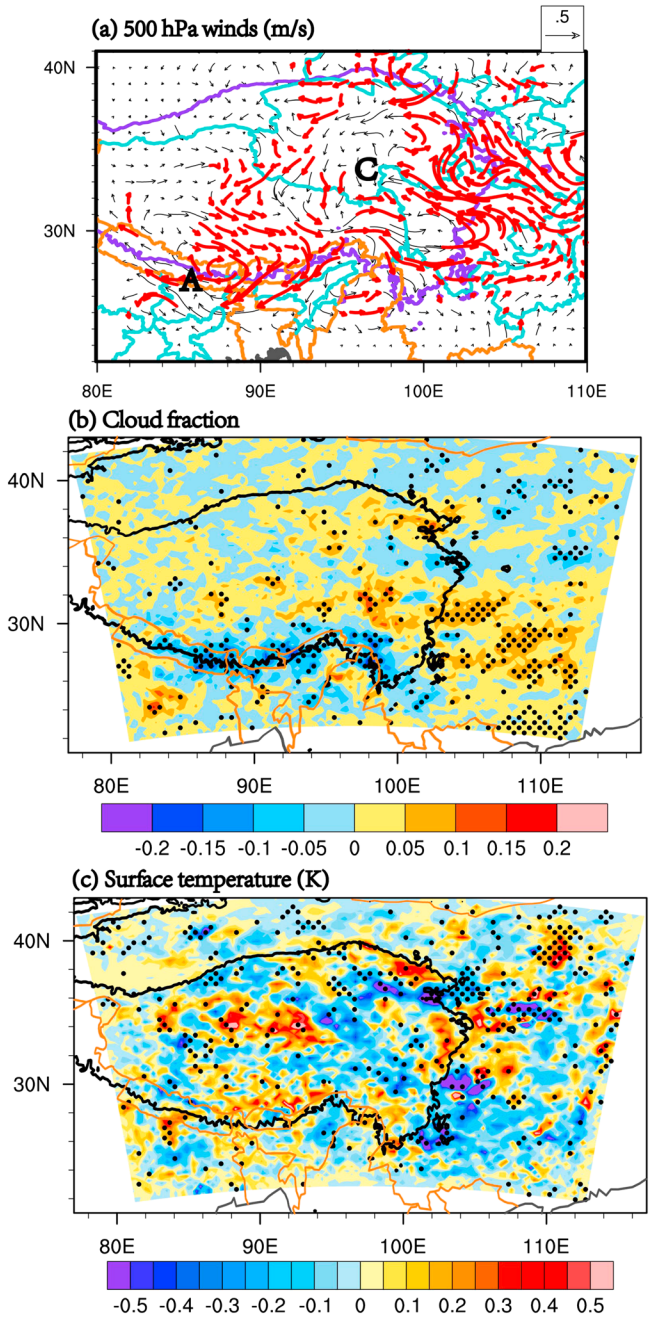

Figure 9. (a) Differences in the winds at 500 hPa between the maximum and minimum BC runs averaged during 28 June to 6 July 2008 in the WRF model (>90% significance level shown as red arrows) (units: m/s). Differences in (b) cloud fraction and (c) surface temperature between the maximum and minimum black carbon runs in the Weather Research and Forecasting model (>90% confidence levels are shown as dots).

4.2.2. WRF Simulations

The WRF simulation is driven by meteorological forcing for the period 28 June to 6 July 2008 (9 days). Two experiments are carried out. The first experiment is a control run to evaluate the performance of the simulated circulations in this ISV event using prescribed aerosol forcing on 28 June 2008. The second simulation adopts the approach of Chen and Wang (2016) studying the response of the sea surface temperature to shortwave forcing attributed to changes in the concentration of sulfate aerosols. The 9-day (28 June to 6 July 2008) simulation cycles are repeated 20 times each under minimum and maximum BC conditions. The minimum and maximum BC conditions are similar to those defined in section 3.1. Repeating the integration 20 times forces the model to reach a quasi-equilibrium state. The following results are based on the average of the last 10 cycles of the 9-day mean state. The sensitivity experiments show that the atmospheric response to the radiative effects of BC are statistically significant. The difference is compared with the significance estimation of the minimum BC run using Student's *t* test and a significance level of 90%.

Figure 8a shows that an LLC over the SETP is the most distinguishable observed feature if we compare the difference in circulation between 28 June and 2 July 2008. The LLC represents the key developing circulation anomaly in the transition from the dry phase to the wet phase during with this ISV event over the SETP. The results show that this LLC can be reproduced well in the control run for the period 28 June to 6 July 2008 (Figure 8b).

Figure 9a shows the statistically significant changes in circulation in the second experiment. The most noticeable response is a significant LLC anomaly over the TP. The locations and magnitudes (0.5 m/s) of this LLC anomaly are similar to the LBM results (Figure 6f). This indicates that the LLC over the SETP is the key circulation anomaly (0.5 m/s) in the transition period and is intensified by nearly 10% (0.5/5) relative to the natural magnitude (5 m/s) of wind variation measured by wind speed.

Figure 9b shows the corresponding change in cloud fraction at lower levels of the TP (400–550 hPa). Since no indirect effect of aerosol involves the cloud process, the cloud change is primarily ascribed to dynamical processes due to BC radiative forcing and associated feedback. The cloud fraction is evidently increased by 5–15% over the SETP. The domain that cloud fraction increases is almost consistent with the LLC region, because the LLC corresponds to enhanced upward motion and low-level moisture convergence that cause the increased fraction of cloud.

A cooling anomaly of 0.2–0.5° is detected over the SETP region (Figure 9c), which could be ascribed to one of the following two reasons. One is the direct radiative effect of the absorption by BC, which reduces the amount of downward shortwave radiation reaching the surface as shown in Figure 5b. The other is that the increased cloud fraction may reduce the downward shortwave radiation, which indirectly causes surface cooling. (Figures 9b and 9c). Because surface cooling may stabilize the boundary layer and suppress the development of the LLC, this indicates that the atmospheric radiative effect of BC should generate a stronger LLC anomaly than that shown here if without the feedback of surface cooling. The results also suggest that the changes in circulation are mainly due to atmospheric radiative warming by BC and that surface radiative cooling plays only a minor part.

We further examine the precipitation response over the core region of the TP because we assume that the local rainfall should increase due to the enhanced LLC over the SETP. Figure 10a shows that positive

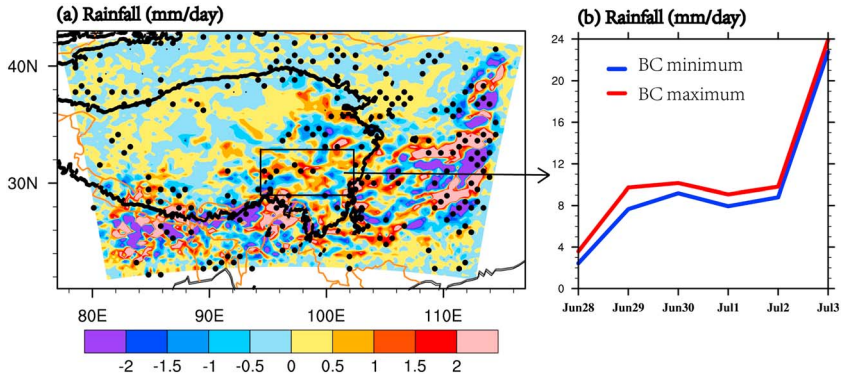

Figure 10. (a) Total difference in rainfall between the maximum and minimum BC concentration runs averaged during 28 June–6 July 2008 in the Weather Research and Forecasting model (>90% confidence levels are shown as dots). (b) Domain-averaged rainfall time series (black box in part (a)) at the transition in the maximum and minimum BC concentration runs. BC = black carbon.

rainfall signals can be detected particularly over south eastern portion of the core region but not uniform over SETP. The mean amount of rainfall increases by nearly 6% relative to the variation in developing phase of rainfall averaged over the positive anomalous rainfall domain of SETP (Figure 10b). The intensity of rainfall over the TP may therefore be influenced by changes in the spatial distribution of BC. These results also indicate it is necessary to study the adjustment effects between BC and clouds.

5. Conclusion and Discussion

5.1. Conclusion

There have been few reported studies of the coupling and feedback between circulation and aerosols on short timescales, particularly on intraseasonal timescales. Based on a typical intraseasonal (quasi-9-day) event over the SETP in the summer of 2008, we investigated the variation of BC concentration induced by changes in circulation and its effects on atmospheric circulation using observations and sensitivity simulations. In observation, the development of an LLC is the dominant feature over the SETP at the transition from the dry phase to the wet phase. The LLC accompanies strong upward motion and convergence toward the TP at lower levels, which increases the concentrations of BC, particularly over the southern and eastern TP. The increased concentrations of BC warm the atmosphere, particularly in the lower levels, due to the absorption of radiation. Atmospheric warming is increased over the TP in particular as a result of the thinner air in this high-elevation region. As a feedback to the radiative heating caused by BC, a weak but statistically significant LLC anomaly is induced over the SETP in both the LBM and WRF simulations. The cloud cover is also increased due to enhanced upward motion and increased amounts of moisture caused directly by the LLC. The surface temperature is reduced over the SETP by the absorption of radiation by BC within the atmosphere and by the increased cloud cover induced by the anomalous LLC. Precipitation is also slightly increased over the SETP as a response. This study also suggests that radiative warming of the atmosphere dominates the changes in circulation, whereas surface radiative cooling plays only a minor part in this case study. The above-mentioned interaction between BC concentrations and the meteorological conditions in this case study is summarized in Figure 11.

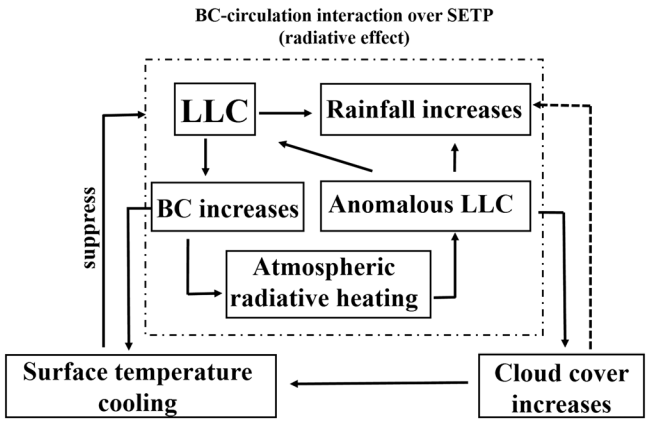

Figure 11. Schematic diagram for the interaction between BC and circulation over the SETP in the boreal summer. Solid arrows are verified results, and the dotted arrows denote results that need to be further verified. BC = black carbon; SETP = southeastern Tibetan Plateau.

5.2. Discussion

There are several issues worthy of further investigation. This work only studied the direct radiative effects of BC aerosols. The variations in cloud cover are only caused by circulation anomalies induced by BC in this

study. However, there are plenty of cloud over the TP in summer, including cumulus (Li et al., 2016), stratus (Yu et al., 2004), and cirrus (Chen & Liu, 2005; He et al., 2013; Kodama et al., 2008) clouds. Therefore, the indirect effects of aerosols may have a more considerable effect on ISVs over the TP, although the climate adjustment effect currently has a larger uncertainty (Stocker, 2014), especially over the TP where clouds usually consist of a mixed phase of water and ice. The WRF model (version 3.6.1) coupled with the physics-based two-moment microphysical scheme model used here has the ability to study the indirect effects of aerosols on meteorological conditions (e.g., Chen et al., 2015). We plan to use this model to study intraseasonal aerosol-meteorology coupling, including the indirect effects of aerosols over the TP, in future work. The radiative properties of BC actually vary during aging (e.g., He et al., 2015) and also depend on different mixing states (e.g., Zhuang et al., 2013), but these were not considered in this study.

This numerical experiment only considered the variation in BC, although sources of dust and sulfate/organic carbon also exist in the surrounding areas. For example, dust over the Taklimakan Desert (Xia et al., 2008), the Tarim Basin, the Gobi Desert, northwestern India and the Middle East (Huang et al., 2007; Kopacz et al., 2011; Liu et al., 2008) can be transported to the TP. The ISV of the circulation could also change the spatial distribution of these other aerosols, although their concentration variation is not consistent between the two aerosol reanalysis data sets available for this case study. The changes in the concentrations of other aerosols are assumed to influence circulation by absorptive heating or radiative cooling, which will be investigated in the future using more reliable data sets.

Our results show a climate-sensitive response to two types of spatial patterns of BC concentrations over the TP induced by an ISV event on a short-term timescale. Previous studies have found that different loadings of aerosols can affect the transition from dry to wet phases in the ISV of the Indian summer monsoon and the Madden-Julian oscillation. Recent work (Chen et al., 2017) has shown the effect of aerosol loadings on the ISV of the East Asian monsoon. It should be noted that we used prescribed aerosols concentrations in the simulation to investigate the effect of different concentrations of BC on the short-term circulation, but we did not include the real day-by-day variation in aerosol concentrations. Thus, the response of the circulation in the idealized experiment might be overestimated because we only used two extreme concentrations of BC in this study (e.g., He et al., 2014). The most important implication of this study is that it is imperative to consider aerosol-circulation coupling to advance the prediction of short-term changes in circulation.

Acknowledgments
This work is supported by the National Natural Science Foundation of China (41775071, 41621061, and 41675100). This study is also supported by funds from the National Key Research and Development Program–Global Change and Mitigation Project: Global change risk of population and economic system: mechanism and assessment (grant 2016YFA0602401). The gridded stations data are from the China Meteorological Administration (IP: 59.64.36.30: ~/mnt/storage-3/CN05.1_1961-2015). The ERA-Interim data can be freely downloaded from http://apps.ecmwf.int/datasets/data/interim-full-daily/levtype=sfc/. The MACC-II data set can be accessed on http://apps.ecmwf.int/datasets/data/macc-reanalysis/levtype=sfc/. The MERRA 2 data set can be accessed on https://daac.gsfc.nasa.gov/datasets?page=1&keywords=merra-2.

References

Benedetti, A., Morcrette, J. -J., Boucher, O., Dethof, A., Engelen, R. J., Fisher, M., et al. (2009). Aerosol analysis and forecast in the European Centre for Medium-Range Weather Forecasts Integrated Forecast System: 2. Data assimilation. *Journal of Geophysical Research*, *114*, D13205. https://doi.org/10.1029/2008JD011115

Bucci, S., Cagnazzo, C., Cairo, F., Di Liberto, L., & Fierli, F. (2014). Aerosol variability and atmospheric transport in the Himalayan region from CALIOP 2007–2010 observations. *Atmospheric Chemistry and Physics*, *14*(9), 4369–4381. https://doi.org/10.5194/acp-14-4369-2014

Chen, B., & Liu, X. (2005). Seasonal migration of cirrus clouds over the Asian Monsoon regions and the Tibetan Plateau measured from MODIS/Terra. *Geophysical Research Letters*, *32*, L01804. https://doi.org/10.1029/2004GL020868

Chen, F., & Dudhia, J. (2001). Coupling an advanced land surface hydrology model with the Penn State-NCAR MM5 modeling system. Part I: model implementation and sensitivity. *Monthly Weather Review*, *129*(4), 569–585.5. https://doi.org/10.1175/1520-0493(2001)129<056<0569:CAALSH>SH>2.0.CO;2;2

Chen, G. X., & Wang, W. C. (2016). Aerosol–stratocumulus–radiation interactions over the southeast Pacific: Implications to the underlying air–sea coupling. *Journal of the Atmospheric Sciences*, *73*(7), 2759–2771. https://doi.org/10.1175/JAS-D-15-0277.1

Chen, G. X., Wang, W. C., & Chen, J. P. (2015). Aerosol-stratocumulus-radiation interactions over the southeast Pacific. *Journal of the Atmospheric Sciences*, *72*(7), 2612–2621. https://doi.org/10.1175/JAS-D-14-0319.1

Chen, G. X., Yang, J., Bao, Q., & Wang, W. C. (2017). Intraseasonal responses of the East Asia summer rainfall to anthropogenic aerosol climate forcing. *Climate Dynamics*. https://doi.org/10.1007/s00382-017-3691-0

Cheng, C. T., Wang, W. C., & Chen, J. P. (2007). A modelling study of aerosol impacts on cloud microphysics and radiative properties. *Quarterly Journal of the Royal Meteorological Society*, *133*(623), 283–297. https://doi.org/10.1002/qj.25

Cheng, C. T., Wang, W. C., & Chen, J. P. (2010). Simulation of the effects of increasing cloud condensation nuclei on mixed-phase clouds and precipitation of a front system. *Atmospheric Research*, *96*(2–3), 461–476. https://doi.org/10.1016/j.atmosres.2010.02.005

Chin, M., Ginoux, P., Kinne, S., Torres, O., Holben, B. N., Duncan, B. N., et al. (2002). Tropospheric aerosol optical thickness from the GOCART model and comparisons with satellite and sun photometer measurements. *Journal of the Atmospheric Sciences*, *59*(3), 461–483. https://doi.org/10.1175/1520-0469(2002)059<0461:TAOTFT>2.0.CO;2

Dee, D. P., Uppala, S. M., Simmons, A. J., Berrisford, P., Poli, P., Kobayashi, S., et al. (2011). The ERA-interim reanalysis: Configuration and performance of the data assimilation system. *Quarterly Journal of the Royal Meteorological Society*, *137*(656), 553–597. https://doi.org/10.1002/qj.828

Duan, A. M., Wu, G. X., Liu, Y. M., Ma, Y. M., & Zhao, P. (2012). Weather and climate effects of the Tibetan Plateau. *Advances in Atmospheric Sciences*, *29*(5), 978–992. https://doi.org/10.1007/s00376-012-1220-y

Endo, N., Ueno, K., & Yasunari, T. (1994). Seasonal change of the troposphere in the early summer of 1993 over the central Tibet observed in Tanggula mountains. *Bulletin of Glacier Research*, *12*, 25–30.

He, C., Li, Q. B., Liou, K. N., Takano, Y., Gu, Y., Qi, L., et al. (2014). Black carbon radiative forcing over the Tibetan Plateau. *Geophysical Research Letters*, *41*, 7806–7813. https://doi.org/10.1002/2014gl062191

He, C., Liou, K. N., Takano, Y., Zhang, R., Levy Zamora, M., Yang, P., et al. (2015). Variation of the radiative properties during black carbon aging: Theoretical and experimental intercomparison. *Atmospheric Chemistry and Physics*, *15*(20), 11,967–11,980. https://doi.org/10.5194/acp-15-11967-2015

He, Q. S., Li, C. C., Ma, J. Z., Wang, H. Q., Shi, G. M., Liang, Z. R., et al. (2013). The properties and formation of cirrus clouds over the Tibetan Plateau based on summertime Lidar measurements. *Journal of the Atmospheric Sciences*, *70*(3), 901–915. https://doi.org/10.1175/JAS-D-12-0171.1

Hong, S. Y., Noh, Y., & Dudhia, J. (2006). A new vertical diffusion package with an explicit treatment of entrainment processes. *Monthly Weather Review*, *134*(9), 2318–2341. https://doi.org/10.1175/MWR3199.1

Hu, W. T., Duan, A. M., Li, Y., & He, B. (2016). The Intraseasonal oscillation of eastern Tibetan Plateau precipitation in response to the summer Eurasian wave train. *Journal of Climate*, *29*(20), 7215–7230. https://doi.org/10.1175/JCLI-D-15-0620.1

Huang, J. P., Minnis, P., Yi, Y. H., Tang, Q., Wang, X., Hu, Y. X., et al. (2007). Summer dust aerosols detected from CALIPSO over the Tibetan Plateau. *Geophysical Research Letters*, *34*, L18805. https://doi.org/10.1029/2007GL029938

Iacono, M. J., Delamere, J. S., Mlawer, E. J., Shephard, M. W., Clough, S. A., & Collins, W. D. (2008). Radiative forcing by long-lived greenhouse gases: Calculations with the AER radiative transfer models. *Journal of Geophysical Research*, *113*, D13103. https://doi.org/10.1029/2008JD009944

Kain, J. S. (2004). The Kain-Fritsch convective parameterization: An update. *Journal of Applied Meteorology*, *43*(1), 170–181. https://doi.org/10.1175/1520-0450(2004)043<0170:TKCPAU>2.0.CO;2

Kodama, Y. M., Egawa, K., & Takahashi, M. (2008). Medium-scale tropopausal waves visualized by upper-level clouds to the east of the Tibetan Plateau. *Journal of the Meteorological Society of Japan*, *86*(2), 279–295. https://doi.org/10.2151/jmsj.86.279

Kopacz, M., Mauzerall, D. L., Wang, J., Leibensperger, E. M., Henze, D. K., & Singh, K. (2011). Origin and radiative forcing of black carbon transported to the Himalayas and Tibetan Plateau. *Atmospheric Chemistry and Physics*, *11*(6), 2837–2852. https://doi.org/10.5194/acp-11-2837-2011

Lau, K. M., Kim, M. K., & Kim, K. M. (2006). Asian summer monsoon anomalies induced by aerosol direct forcing: The role of the Tibetan Plateau. *Climate Dynamics*, *26*(7–8), 855–864. https://doi.org/10.1007/s00382-006-0114-z

Lau, W. K. M., Kim, M. K., Kim, K. M., & Lee, W. S. (2010). Enhanced surface warming and accelerated snow melt in the Himalayas and Tibetan Plateau induced by absorbing aerosols. *Environmental Research Letters*, *5*(2), 025204. https://doi.org/10.1088/1748-9326/5/2/025204

Lee, W. L., Liou, K. N., He, C. L., Liang, H. C., Wang, T. C., Li, Q. B., et al. (2016). Impact of absorbing aerosol deposition on snow albedo reduction over the southern Tibetan plateau based on satellite observations. *Theoretical and Applied Climatology*, *129*(3–4), 1373–1382. https://doi.org/10.1007/s00704-016-1860-4

Li, Z. Q., Lau, W. K. M., Ramanathan, V., Wu, G., Ding, Y., Manoj, M. G., et al. (2016). Aerosol and monsoon climate interactions over Asia. *Reviews of Geophysics*, *54*, 866–929. https://doi.org/10.1002/2015RG000500

Liu, Y. M., Hoskins, B. J., & Blackburn, M. (2007). Impact of Tibetan orography oscillation and heating on the summer flow over Asia. *Journal of the Meteorological Society of Japan*, *85B*, 1–19. https://doi.org/10.2151/jmsj.85B.1

Liu, Z. Y., Liu, D., Huang, J. P., Vaughan, M., Uno, I., Sugimoto, N., et al. (2008). Airborne dust distributions over the Tibetan Plateau and surrounding areas derived from the first year of CALIPSO Lidar observations. *Atmospheric Chemistry and Physics*, *8*(16), 5045–5060. https://doi.org/10.5194/acp-8-5045-2008

Manoj, M. G., Devara, P. C. S., Safai, P. D., & Goswami, B. N. (2011). Absorbing aerosols facilitate transition of Indian monsoon breaks to active spell. *Climate Dynamics*, *37*(11–12), 2181–2198. https://doi.org/10.1007/s00382-010-0971-3

Ming, J., Xiao, C. D., Cachier, H., Qin, D. H., Qin, X., Li, Z. Q., & et al. (2009). Black carbon (BC) in the snow of glaciers in west China and its potential effects on albedos. *Atmospheric Research*, *92*(1), 114–123. https://doi.org/10.1016/j.atmosres.2008.09.007

Molod, A., Takacs, L., Suarez, M., & Bacmeister, J. (2015). Development of the GEOS-5 atmospheric general circulation model: Evolution from MERRA to MERRA2. *Geoscientific Model Development*, *8*(5), 1339–1356. https://doi.org/10.5194/gmd-8-1339-2015

Monin, A. S., & Obukhov, A. M. (1954). Basic laws of turbulent mixing in the surface layer of the atmosphere. *Trudy Geofizicheskogo Instituta, Akademiya Nauk SSSR*, *24*(151), 163–187.

Morcrette, J.-J., Boucher, O., Jones, L., Salmond, D., Bechtold, P., Benedetti, A., et al. (2009). Aerosol analysis and forecast in the European Centre for Medium-Range Weather Forecasts Integrated Forecast System: Forward modelling. *Journal of Geophysical Research*, *114*, D06206. https://doi.org/10.1029/2008JD011235

Myhre, G., Samset, B. H., Schulz, M., Balkanski, Y., Bauer, S., Berntsen, T. K., et al. (2013). Radiative forcing of the direct aerosol effect from AeroCom Phase II simulations. *Atmospheric Chemistry and Physics*, *13*(4), 1853–1877. https://doi.org/10.5194/acp-13-1853-2013

Peuch, V. H., Engelen, R., Calnan, R., Lambert, J.-C., Rudder, A., Tarrason, L., et al. (Eds.). (2014). *MACC-II final report: Monitoring Atmospheric Composition and Climate-Interim Implementation* (the European Union's Framework Programme under grant agreement number 283576). Retrieved from https://atmosphere.copernicus.eu

Qian, Y. P., Flanner, M. G., Leung, L. R., & Wang, W. (2011). Sensitivity studies on the impacts of Tibetan plateau snowpack pollution on the Asian hydrological cycle and monsoon climate. *Atmospheric Chemistry and Physics*, *11*(5), 1929–1948. https://doi.org/10.5194/acp-11-1929-2011

Rienecker, M. M., Suarez, M. J., Rienecker, M. M., Todling, R., Bacmeister, J., Takacs, L., et al. (2008). The GEOS-5 Data Assimilation System—Documentation of Versions 5.0.1 and 5.1.0, and 5.2.0. NASA Technical Report Series on Global Modeling and Data Assimilation, NASA/TM-2008-104606, 27, 92 pp.

Samset, B. H., Myhre, G., Schulz, M., Balkanski, Y., Bauer, S., Berntsen, T. K., et al. (2013). Black carbon vertical profiles strongly affect its radiative forcing uncertainty. *Atmospheric Chemistry and Physics*, *13*(5), 2423–2434. https://doi.org/10.5194/acp-13-2423-2013

Simmons, A., Uppala, S., Dee, D., & Kobayashi, S. (2007). ERA-Interim: New ECMWF reanalysis products from 1989 onwards. *ECMWF Newsl*, *110*, 25–35. https://doi.org/10.21957/pocnex23c6

Stocker, T. (2014). *Climate change 2013: The physical science basis: Working group I contribution to the fifth assessment report of the Intergovernmental Panel on Climate Change*. Cambridge: Cambridge University Press.

Tao, S. Y., & Ding, Y. H. (1981). Observational evidence of the influence of the Qinghai-Xizang (Tibet) plateau on the occurrence of heavy rain and severe convective storms in China. *Bulletin of the American Meteorological Society*, *62*(1), 23–30. https://doi.org/10.1175/1520-0477(1981)062<0023:OEOTIO>2.0.CO;2

Thompson, G., & Eidhammer, T. (2014). A study of aerosol impacts on clouds and precipitation development in a large winter cyclone. *Journal of the Atmospheric Sciences*, *71*(10), 3636–3658. https://doi.org/10.1175/JAS-D-13-0305.1

Tian, B. J., Waliser, D. E., Kahn, R. A., Li, Q. B., Yung, Y. L., Tyranowski, T., et al. (2008). Does the Madden-Julian oscillation influence aerosol variability? *Journal of Geophysical Research*, *113*, D12215. https://doi.org/10.1029/2007JD009372

Wang, M. R., & Duan, A. M. (2015). Quasi-biweekly oscillation over the Tibetan Plateau and its link with the Asian summer monsoon. *Journal of Climate*, *28*(12), 4921–4940. https://doi.org/10.1175/JCLI-D-14-00658.1

Watanabe, M., & Kimoto, M. (2000). Atmosphere-ocean thermal coupling in the North Atlantic: A positive feedback. *Quarterly Journal of the Royal Meteorological Society*, *126*(570), 3343–3369. https://doi.org/10.1256/smsqj.57016

Wu, G. X., Duan, A. M., Liu, Y. M., Mao, J. Y., Ren, R. C., Bao, Q., et al. (2015). Tibetan Plateau climate dynamics: Recent research progress and outlook. *National Science Review*, *2*(1), 100–116. https://doi.org/10.1093/nsr/nwu045

Wu, G. X., Liu, Y. M., Zhu, X., Li, W., Ren, R. C., Duan, A. M., & et al. (2009). Multi-scale forcing and the formation of subtropical desert and monsoon. *Annales Geophysicae*, *27*(9), 3631–3644. https://doi.org/10.5194/angeo-27-3631-2009

Wu, J., & Gao, X. J. (2013). A gridded daily observation dataset over China region and comparison with the other datasets. *Chinese Journal of Geophysics*, *56*(4), 1102–1111. (in Chinese)

Xia, X., Zong, X., Cong, Z., Chen, H., Kang, S., & Wang, P. (2011). Baseline continental aerosol over the central Tibetan plateau and a case study of aerosol transport from South Asia. *Atmospheric Environment*, *45*(39), 7370–7378. https://doi.org/10.1016/j.atmosenv.2011.07.067

Xia, X. G., Wang, P. C., Wang, Y. S., Li, Z. Q., Xin, J. Y., Liu, J., & et al. (2008). Aerosol optical depth over the Tibetan Plateau and its relation to aerosols over the Taklimakan Desert. *Geophysical Research Letters*, *35*, L16804. https://doi.org/10.1029/2008GL034981

Yamada, T., & Uyeda, H. (2006). Transition of the rainfall characteristics related to the moistening of the land surface over the central Tibetan Plateau during the summer of 1998. *Monthly Weather Review*, *134*(11), 3230–3247. https://doi.org/10.1175/MWR3235.1

Yang, J., Bao, Q., Gong, D. Y., & Wang, B. (2014). Distinct quasi-biweekly variations of the subtropical East Asian monsoon during early and late summers. *Climate Dynamics*, *42*(5–6), 1469–1486. https://doi.org/10.1007/s00382-013-1728-6

Yang, J., Bao, Q., Wang, B., He, H. Z., Gao, M. N., & Gong, D. Y. (2016). Characterizing two types of transient intraseasonal oscillations in the eastern Tibetan Plateau summer rainfall. *Climate Dynamics*, *48*(5–6), 1749–1768. https://doi.org/10.1007/s00382-016-3170-z

Yang, J., Wang, B., Wang, B., & Bao, Q. (2010). Biweekly and 21–30 day variabilities of the subtropical East Asian monsoon over the lower reach of Yangtze River basin. *Journal of Climate*, *23*(5), 1146–1159. https://doi.org/10.1175/2009JCLI3005.1

Yeh, T. -C., Lo, S. -W., & Chu, P.-C. (1957). The wind structure and heat balance in the lower troposphere over Tibetan Plateau and its surroundings. *Acta Meteorologica Sinica*, *28*, 108–121.

Yu, H., Dickinson, R. E., Chin, M., Kaufman, Y. J., Zhou, M., Zhou, L., et al. (2004). The direct radiative effect of aerosols as determined from a combination of MODIS retrievals and GOCART simulations. *Journal of Geophysical Research*, *109*, D03206. https://doi.org/10.1029/2003JD003914

Zhan, R. F., & Li, J. P. (2008). Validation and characteristics of upper tropospheric water vapor over the Tibetan Plateau from AIRS satellite retrieval (in Chinese). *Chinese Journal of Atmosphere Science*, *32*(2), 242–260.

Zhang, P. F., Li, G. P., Fu, X. H., Liu, Y. M., & Li, L. F. (2014). Clustering of Tibetan Plateau vortices by 10-30-day intraseasonal oscillation. *Monthly Weather Review*, *142*(1), 290–300. https://doi.org/10.1175/MWR-D-13-00137.1

Zhao, Z. Z., Cao, J. J., Shen, Z. X., Xu, B. Q., Zhu, C. S., Chen, L.-W. A., et al. (2013). Aerosol particles at a high-altitude site on the southeast Tibetan Plateau, China: Implications for pollution transport from South Asia. *Journal of Geophysical Research: Atmospheres*, *118*, 11,360–11,375. https://doi.org/10.1002/jgrd.50599

Zhuang, B. L., Li, S., Wang, T. J., Deng, J. J., Xie, M., Yin, C. Q., & et al. (2013). Direct radiative forcing and climate effects of anthropogenic aerosols with different mixing states over China. *Atmospheric Environment*, *79*, 349–361. https://doi.org/10.1016/j.atmosenv.2013.07.004